Conformational effects on the torsional barriers in m-methylanisole studied by microwave spectroscopy

Lynn Ferres, Wolfgang Stahl, Ha Vinh Lam Nguyen

Conformational effects on the torsional barriers in m-methylanisole studied by microwave spectroscopy

Lynn Ferres, Wolfgang Stahl, and Ha Vinh Lam Nguyen

Citation: The Journal of Chemical Physics **148**, 124304 (2018); doi: 10.1063/1.5016273
View online: https://doi.org/10.1063/1.5016273
View Table of Contents: http://aip.scitation.org/toc/jcp/148/12
Published by the American Institute of Physics

Conformational effects on the torsional barriers in *m*-methylanisole studied by microwave spectroscopy

Lynn Ferres,[1] Wolfgang Stahl,[1] and Ha Vinh Lam Nguyen[2,a)]
[1]*Institute of Physical Chemistry, RWTH Aachen University, Landoltweg 2, D-52074 Aachen, Germany*
[2]*Laboratoire Interuniversitaire des Systèmes Atmosphériques (LISA), CNRS UMR 7583, Université Paris-Est Créteil, Université Paris Diderot, Institut Pierre Simon Laplace, 61 Avenue du Général de Gaulle, F-94010 Créteil, France*

(Received 17 November 2017; accepted 27 February 2018; published online 23 March 2018)

The microwave spectrum of *m*-methylanisole (also known as 3-methylanisole, or 3-methoxytoluene) was measured using a pulsed molecular jet Fourier transform microwave spectrometer operating in the frequency range of 2–26.5 GHz. Quantum chemical calculations predicted two conformers with the methoxy group in *trans* or *cis* position related to the ring methyl group, both of which were assigned in the experimental spectrum. Due to the internal rotation of the ring methyl group, all rotational transitions introduced large A-E splittings up to several GHz, which were analyzed with a newly developed program, called *aixPAM*, working in the principal axis system. There are significant differences in the V_3 potential barriers of 55.7693(90) cm^{-1} and 36.6342(84) cm^{-1} determined by fitting 223 and 320 torsional components of the *cis* and the *trans* conformer, respectively. These values were compared with those found in other *m*-substituted toluenes as well as in *o*- and *p*-methylanisole. A comparison between the *aixPAM* and the *XIAM* code (using a combined axis system) was also performed. *Published by AIP Publishing.* https://doi.org/10.1063/1.5016273

I. INTRODUCTION

Rotational transitions of a molecule with internal rotation of a methyl group feature splittings into torsional components and can no longer be treated using a rigid-rotor model. A number of programs have been developed to treat this problem; among them are *IAM*,[1] *XIAM*,[2] *BELGI-C_s*[3] and *BELGI-C_1*,[4] *Erham*,[5] and *RAM36*.[6] All of them use a rigid frame-rigid top model[7] as a theoretical background, which is supplemented by a number of higher order (effective) terms, including centrifugal distortion of both the frame and the top in the Hamiltonian. On the other hand, they differ from each other by their methods which are named after the coordinates in use; e.g., the *XIAM* code uses the combined axis method; *Erham* sets up and solves an **E**ffective **R**otational **HAM**iltonian; and *BELGI-C_s*, *BELGI-C_1*, as well as *RAM36* use the rho axis method (RAM). The numerical techniques are also different: The Hamiltonian matrices are pre-diagonalized, small matrix elements are neglected, and the matrices are truncated at a given limit.

The program *XIAM* was mostly used in our previous investigations on molecules of different chemical classes, such as methyl butyrate,[8] *N,N*-diethylacetamide,[9] and methyl isobutyl ketone,[10] undergoing internal rotation because it is user-friendly and offers a reasonable compromise of accuracy and speed of the calculations. On the other hand, *XIAM* has its weaknesses in treating internal rotations with low barrier heights, e.g., in the cases of 3-pentin-1-ol,[11] allyl acetate,[12] and *N*-ethylacetamide,[13] where in the fits, standard deviations much larger than measurement accuracy have been observed.

For numerous molecular systems, we compared fits carried out with *XIAM* and *BELGI* in its C_s or C_1 version, where in almost all the cases, *BELGI* yielded a lower standard deviation than *XIAM* with the same data set.[14–16] There were some discussions about the reasons for this observation. A frequently used argument is that only a limited number of parameters can be fitted using *XIAM* in comparison with *BELGI* and that the torsional interactions between different v_t states are not taken into account explicitly. Higher order coupling terms between the internal rotation and the overall rotation cannot be easily implemented in the *XIAM* code to improve the quality of the fit. Sometimes, it is also argued that even if there were more effective terms in *XIAM*, the standard deviation would still be worse than with *BELGI*. The reason is that *XIAM* uses a two-step diagonalization procedure, whereby only one *J*-block is considered in the second diagonalization step and some matrix elements are thus neglected. This truncation could additionally affect the accuracy of the fit.

These discussions induced the authors to write another internal rotation program, called *aixPAM*, where aix stands for Aix-la-Chapelle, the French name of Aachen where the program was written. *m*-methylanisole (MMA) was chosen for the first application of *aixPAM* since two conformers with rather extensive data sets have been recently measured and assigned and because the *XIAM* fits of these data have not achieved measurement accuracy.

Our recent studies on the microwave spectra of *o*-methylanisole (OMA)[17] and *p*-methylanisole (PMA)[18] have

a)Author to whom correspondence should be addressed: lam.nguyen@lisa.u-pec.fr

shown that the ring methyl group undergoes internal rotation with quite different barrier heights of about 444 cm^{-1} and 50 cm^{-1}, respectively, whereas the effect arising from the methoxy methyl group is negligible. It is interesting to compare the respective torsional barriers when the ring methyl group is in *m*-position, because depending on the relative position of the substituents, considerable effects on the torsional barrier height can be observed. There are studies in the literature on the isomers of fluorotoluene,[19–21] cresol,[22–24] and methylbenzaldehyde,[25,26] stating very different barrier heights for the *o*-, *m*-, and *p*-isomers.

A comparison with the barriers of other toluene derivatives with a methyl group in *m*-position is also very interesting. Some previous investigations[17,18,26] have shown that the *o*- and *p*-isomers often possess only one stable conformer because of the sterical hindrance of the *o*-isomer and the structural symmetry of the *p*-isomer. In *m*-substituted toluenes, two conformers are often observed,[25] making these isomers ideally suited to study conformational effects on torsional barriers.

II. THEORETICAL SECTION

A. Quantum chemical calculations

1. Conformational analysis

Before recording the microwave spectrum, quantum chemical calculations were performed to determine the possible conformers of MMA.

By rotating the entire $–OCH_3$ group about the $C_4–O_{11}$ bond (for atom numbering, see Fig. 1), we calculated a potential curve, where the dihedral angle $\beta = \angle(C_5,C_4,O_{11},C_{12})$ was varied in a grid of 10°, while all other geometry parameters were optimized. If not stated otherwise, calculations were carried out at the B3LYP/6-311++G(d,p) level of theory using the *Gaussian09* program package.[27] In almost all the recent investigations, we applied the MP2/6-311++G(d,p) level. However, for molecules containing aromatic rings like phenetole,[28] 2,5-dimethylthiophene,[29] 2-acetyl-5-methylfuran,[30] as well as the isomer OMA[17] of MMA, harmonic frequency calculations yielded one imaginary vibrational mode, which is a bending vibration of the phenyl ring. It is well known that the MP2/6-311++G(d,p) level of theory often yields an imaginary frequency for stable planar ring systems, which has been reported for benzene and arenes.[31] This effect did not occur in calculations using the B3LYP method. Variation of the methods and basis sets in our previous studies on OMA[17] and PMA[18] confirms that the structural parameters do not change significantly and the rotational constants are calculated with sufficient accuracy at the B3LYP/6-311++G(d,p) level.

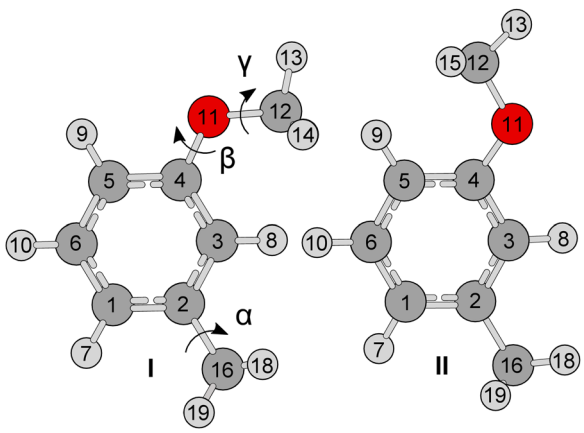

FIG. 1. Molecular structures of the *cis* (I) and the *trans* (II) conformer of MMA optimized at the B3LYP/6-311++G(d,p) level of theory. The dihedral angles are defined as $\alpha = \angle(C_3,C_2,C_{16},H_{18})$, $\beta = \angle(C_5,C_4,O_{11},C_{12})$, and $\gamma = \angle(C_4,O_{11},C_{12},H_{13})$.

The potential curve as a function of β is given in Fig. 2; the Fourier coefficients of the potential function are given in Table S1 (supplementary material). Calculations yield two possible conformers of MMA: the energetically more favorable *trans* conformer at β = 0° and the *cis* conformer at β = 180°. Their fully optimized structures are illustrated in Fig. 1; the Cartesian coordinates are given in Table S2 (supplementary material). Frequency calculations state that both of them are true minima with an energy difference of only 0.40 kJ/mol. We thus expect to observe both conformers in the experimental spectrum.

Optimizations predict the rotational constants $A = 2756.8$ MHz, $B = 1286.6$ MHz, and $C = 887.0$ MHz, as well as the dipole moment components $\mu_a = -0.08$ D, $\mu_b = -1.64$ D, and $\mu_c = 0.00$ D for the *cis* conformer. The respective values for the *trans* conformer are $A = 3537.9$ MHz, $B = 1116.2$ MHz, and $C = 857.7$ MHz, and $\mu_a = 0.67$ D, $\mu_b = 0.73$ D, and $\mu_c = 0.00$ D. Accordingly, for *cis*-MMA, only *b*-type transitions are expected in the microwave spectrum, while *a*-type transitions should also be observable for *trans*-MMA. Finally, anharmonic frequency calculations were carried out to obtain the centrifugal distortion constants.

2. Methyl internal rotations

Potential energy scans generated barrier heights of the ring and the methoxy methyl groups by varying the dihedral

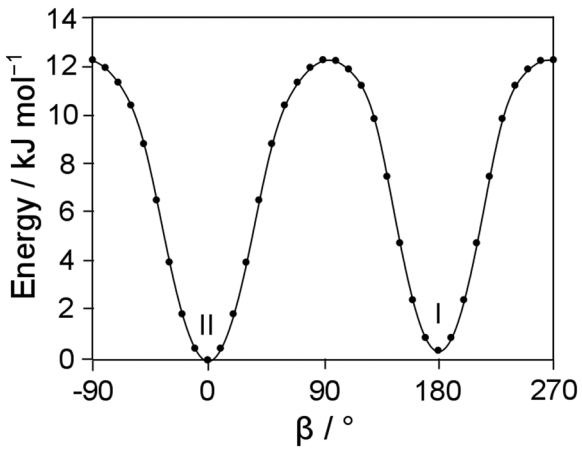

FIG. 2. The potential energy curve of MMA obtained by rotating the methoxy group about the $C_4–O_{11}$ bond by varying the dihedral angle $\beta = \angle(C_5,C_4,O_{11},C_{12})$ in a grid of 10° at the B3LYP/6-311++G(d,p) level of theory. The relative energies with respect to the lowest energy conformation with $E = -386.195\,345\,3$ hartree are given. Two stable C_s conformers found at β = 0° (*trans*) and 180° (*cis*) differ by only 0.40 kJ/mol in energy.

angles $\alpha = \angle(C_3,C_2,C_{16},H_{18})$ and $\gamma = \angle(C_4,O_{11},C_{12},H_{13})$ in a grid of 10°, corresponding to rotations about the C_2–C_{16} and O_{11}–C_{12} bonds, respectively. All other geometry parameters were optimized. Due to the three-fold symmetry of the methyl groups, a rotation of 120° was sufficient. The potential energy curves showing the rotation of the ring methyl group are presented in Fig. 3; the corresponding Fourier coefficients are available in Table S1 (supplementary material). For the *cis* conformer, we found V_3 potentials of 50.13 cm^{-1} for the ring methyl group and 1085.35 cm^{-1} for the methoxy methyl group. The respective values for the *trans* conformer are 32.77 cm^{-1} and 1079.11 cm^{-1}.

Figure 3 indicates that the ring methyl group prefers different orientations in the two conformers of MMA. Taking H_8 as the reference (see Fig. 1), the lowest energy conformations of *cis*-MMA locate two of three hydrogen atoms of the ring methyl group staggered to H_8, corresponding to $\alpha = 60°$, 180°, or 300°. On the contrary, *trans*-MMA favors a conformation with one of the hydrogen atoms eclipsed to H_8, corresponding to $\alpha = 0°$, 120°, or 240°.

The V_3 potential of the methoxy methyl group exceeds 1000 cm^{-1} in both the *cis* and *trans* conformers. Trial two-top calculations using the program *XIAM* predict that torsional splittings arising from the internal rotation of this methyl group are smaller than 5 kHz and thus not resolvable with the spectrometer in use.

Furthermore, a 2D potential energy surface (PES) depending on α and β was calculated by varying these dihedral angles in a grid of 10°. The PES was parameterized with a 2D Fourier expansion based on terms representing the correct symmetry of α and β. The Fourier coefficients are also listed in Table S1 (supplementary material). The PES shown in Fig. 4 clearly indicates the following points: (1) two conformers of MMA exist (I = *cis*-MMA and II = *trans*-MMA), (2) conformer I is higher in energy than conformer II, and (3) the orientation of the ring methyl group depends on the position of the methoxy group.

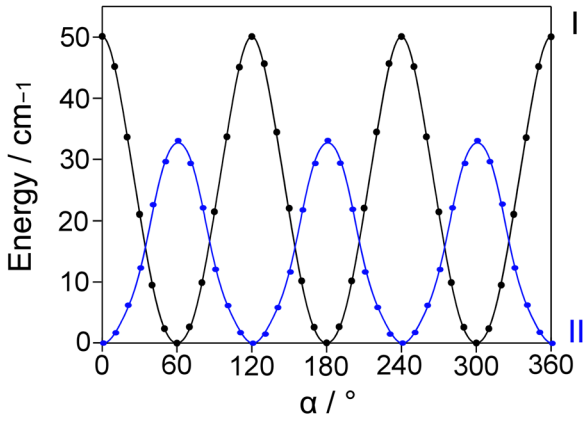

FIG. 3. The potential energy curves for the *cis* (I, black) and the *trans* (II, blue) conformer of MMA obtained by rotating the ring methyl group about the C_2–C_{16} bond. The dihedral angle $\alpha = \angle(C_3,C_2,C_{16},H_{18})$ was varied in a grid of 10°, while all the other molecular parameters were optimized at the B3LYP/6-311++G(d,p) level of theory. Relative energies with respect to the lowest energy conformations with the absolute energies E = −386.195 191 7 and −386.195 345 3 hartree, respectively, are used.

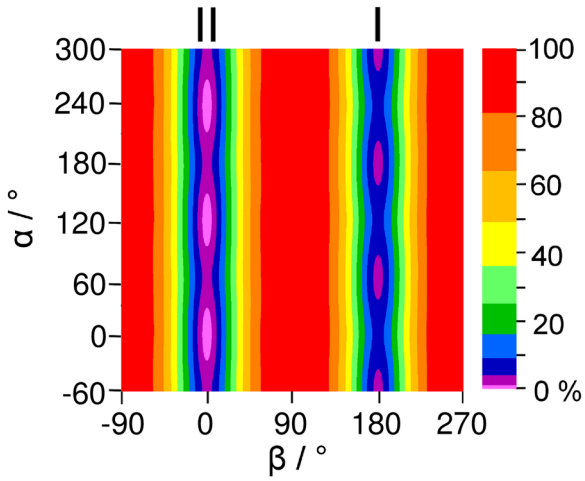

FIG. 4. The potential energy surface (PES) depending on the dihedral angles α and β of MMA calculated at the B3LYP/6-311++G(d,p) level of theory. α and β were varied in a grid of 10°, while all the other parameters were optimized. The numbers in the color code indicate the energy (in percent) relative to the energetic minimum E_{min} = −386.190 522 5 hartree (0%) and the energetic maximum E_{max} = −386.195 345 3 hartree (100%). Note that there are significantly more colors in the lower 50% section. The PES indicates the following: (i) two conformers of MMA exist (I = *cis*-MMA and II = *trans*-MMA), (ii) conformer I is higher in energy than conformer II, and (iii) the orientation of the ring methyl group is different in the two conformers.

B. The *aixPAM* code

The *aixPAM* code is based on the rigid frame-rigid top model. We will briefly describe it here using a notation given in Ref. 32. The Hamiltonian includes the overall rotation, the internal rotation, and Coriolis-like interaction terms. It can be written as

$$H = \frac{1}{2}\vec{P}^{\dagger}\boldsymbol{I}^{-1}\vec{P} + V,$$

with the (transposed) 4-dimensional angular momentum vector $\vec{P}^{\dagger} = \left(P_x, P_y, P_z, p\right)$ and the inertia tensor

$$\boldsymbol{I} = \begin{pmatrix} I_x & 0 & 0 & \lambda_{ix}I_\alpha \\ 0 & I_y & 0 & \lambda_{iy}I_\alpha \\ 0 & 0 & I_z & \lambda_{iz}I_\alpha \\ \lambda_{ix}I_\alpha & \lambda_{iy}I_\alpha & \lambda_{iz}I_\alpha & I_\alpha \end{pmatrix}$$

and the torsional potential

$$V = \sum_n \frac{V_{3n}}{2}\left(1 - \cos 3n\alpha\right).$$

P_g with $g \in \{x, y, z\}$ are the Cartesian components of the overall angular momentum, p is the angular momentum of the internal rotor, I_g are the principal moments of inertia, I_α is the moment of inertia of the internal rotor, and λ_{ig} are the direction cosines between the internal rotor axis i and the principal axes of inertia g. Numerical inversion of $\boldsymbol{I}$ yields

$$\frac{1}{2}\boldsymbol{I}^{-1} = \begin{pmatrix} B'_x & Z_{xy} & Z_{xz} & -Q_x \\ Z_{xy} & B'_y & Z_{yz} & -Q_y \\ Z_{xz} & Z_{yz} & B'_z & -Q_z \\ -Q_x & -Q_y & -Q_z & F \end{pmatrix},$$

and the rigid frame-rigid top Hamiltonian used in *aixPAM* can be written as

$$H = B'_J P^2 + B'_K P_z^2 + B'_- \left(P_x^2 - P_y^2\right) + \sum_{g,g'} Z_{gg'} \left\{P_g, P_{g'}\right\} + Fp^2 - 2\sum_g Q_g P_g p + V,$$

with $B'_J = \frac{B'_x+B'_y}{2}$, $B'_K = B'_z - \frac{B'_x+B'_y}{2}$, $B'_- = \frac{B'_x-B'_y}{2}$, and the anti-commutator $\left\{P_g, P_{g'}\right\} = P_g P_{g'} + P_{g'} P_g$.

Beyond this basic model, centrifugal distortion and effective interaction terms can be added. The Hamiltonian matrix is set up in the principal axis system without pre-diagonalization. A product basis $|\sigma, k\rangle \cdot |J, K\rangle$ of free rotor functions $(2\pi)^{-1}\exp(i(3k+\sigma)\alpha)$ and symmetric top functions is used. Both real and complex matrix elements are allowed. The matrix size is $(2J+1)(2k_{\max}+1)$, with $m_{\max} = 3k_{\max} + \sigma$. The matrices are block-diagonal in the torsional state σ; therefore, one matrix is used for each σ. The matrices are quite large for high J and $k_{\max}$; for example, they are of the size 697×697 for $J = 20$ and $k_{\max} = 8$. However, with modern computers, the time needed for diagonalizing such matrices is only a few seconds. Except for the truncation of the matrix, *aixPAM* does not neglect any other matrix elements and $k_{\max}$ is increased until the fit converges.

An important feature of the *aixPAM* code is the possibility to add effective Hamiltonian terms from the input file. These terms are given as a sum of products of the fundamental operators P^2 (P2), P_z (Pz), $P_+ = P_x + iP_y$ (P+), $P_- = P_x - iP_y$ (P−), p (p), 1 (e0), $e_+ = e^{i3\alpha}$ (e+3), $e_- = e^{-i3\alpha}$ (e−3). The operator codes as they are used in the input file are given in parentheses. P are the angular momenta of the overall rotation, with its components P_x, P_y, P_z, p the angular momentum of the internal rotation about the angle α. The operators 1, $e^{i3\alpha}$, and $e^{-i3\alpha}$ are needed to code the potential operators V_n with n = 3, 6, 9, ... Some examples of effective operators with their corresponding operator descriptions in the input file are given in Table I. We emphasize that in contrast to the *BELGI* code, where all parameters are in the rho axis system, all parameters in *aixPAM* refer to principal axis coordinates.

TABLE I. Some operators and their definitions in the *aixPAM* input file.

Parameter	Operator[a]	Definition[b]		
B'_J	P^2	BJ	1.0	P2
B'_K	P_z^2	BK	1.0	Pz Pz
B'_-	$P_x^2 - P_y^2$	B−	0.5	P+ P+
		B−	0.5	P− P−
Z_{xz}	$\{P_x, P_z\}$	Zxz	0.5	P+ Pz
		Zxz	0.5	P− Pz
		Zxz	0.5	Pz P+
		Zxz	0.5	Pz P−
Q_x	$-2P_x p$	Qx	-1.0	P+ p
		Qx	-1.0	P− p
Q_z	$-2P_z p$	Qz	-2.0	Pz p
Δ_J	$-P^4$	DJ	-1.0	P2 P2
Δ_{JK}	$-P^2 P_z^2$	DJK	-1.0	P2 Pz Pz
Δ_K	$-P_z^4$	DK	-1.0	Pz Pz Pz Pz
δ_J	$-2P^2\left(P_x^2 - P_y^2\right)$	dJ	-1.0	P2 P+ P+
		dJ	-1.0	P2 P− P−
δ_K	$-\left\{P_z^2, \left(P_x^2 - P_y^2\right)\right\}$	dK	-0.5	Pz Pz P+ P+
		dK	-0.5	Pz Pz P− P−
		dK	-0.5	P+ P+ Pz Pz
		dK	-0.5	P− P− Pz Pz
F	p^2	F	1.0	p p
V_3	$\frac{1}{2}(1 - \cos 3\alpha)$	V3	0.5	e0
		V3	-0.25	e+3
		V3	-0.25	e−3
V_6	$\frac{1}{2}(1 - \cos 6\alpha)$	V6	0.5	e0
		V6	-0.25	e+3 e+3
		V6	-0.25	e−3 e−3
D_{mJ}	$P^2 p^2$	DmJ	1.0	P2 p p
D_{mK}	$P_z^2 p^2$	DmK	1.0	Pz Pz p p
V_J	$P^2(1 - \cos 3\alpha)$	FJ	0.5	P2
		FJ	-0.25	P2 e+3
		FJ	-0.25	P2 e−3
V_K	$P_z^2(1 - \cos 3\alpha)$	FK	0.5	Pz Pz
		FK	-0.25	Pz Pz e+3
		FK	-0.25	Pz Pz e−3
V_-	$\left(P_x^2 - P_y^2\right)(1 - \cos 3\alpha)$	F−	0.5	P+ P+
		F−	0.5	P− P−
		F−	-0.25	P+ P+ e+3
		F−	-0.25	P+ P+ e−3
		F−	-0.25	P− P− e+3
		F−	-0.25	P− P− e−3

[a]Anti-commutators are written as $\{u, v\} = uv + vu$.

[b]The fundamental operators are given in the text. Example: The operator associated with V_3 translates to $0.5 - 0.25e^{i3\alpha} - 0.25e^{-i3\alpha} = 0.5(1 - \cos 3\alpha)$.

III. EXPERIMENTAL SECTION

A. Measurements

MMA, purchased from TCI, Eschborn, Germany, has a stated purity of 98% and was used without further purification. The colorless liquid with a typical aromatic smell was placed on a pipe cleaner in a stainless steel tube upstream the nozzle. Under a helium stream at a backing pressure of 2 bars, the helium-MMA mixture was expanded into the vacuum chamber. The spectra were recorded using a supersonic jet Fourier transform microwave spectrometer operating in the frequency range of 2-26.5 GHz.[33] At first, a broadband scan from 8.5 to 16.0 GHz was carried out, where overlapping spectral segments were recorded in a step size of 0.25 MHz. All lines from the scans were remeasured in higher resolution, where they appear as doublets because of the Doppler effect. A portion of the broadband scan is shown in Fig. 5, and a typical measurement at high resolution is shown in Fig. 6. Some intense lines can be measured with an accuracy of 2 kHz, but in most cases, the line widths are larger due to unresolved splittings arising from the internal rotation of the methoxy methyl group and also due to proton spin-spin and spin-rotation coupling, resulting in a measurement accuracy of about 4 kHz. In all fits carried out in the present work, all lines were equally weighted.

B. Spectrum assignment

Quantum chemical calculations have shown that the *trans* conformer is lower in energy than the *cis* conformer (see Sec. II A 1). Additionally, only for this conformer, *a*-type tran-

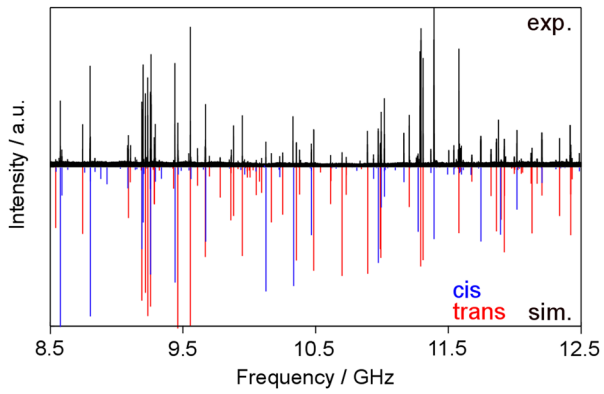

FIG. 5. A portion of the broadband scan of MMA from 8.5 to 12.5 GHz. The experimental spectrum is the upper trace. The lower trace indicates the theoretical spectrum of the *cis* (in blue) and the *trans* (in red) conformer predicted using the molecular parameters deduced from the program *aixPAM*.

sitions, which can often be assigned easily due to their characteristic patterns, are predicted to be observable. Therefore, we began our assignment with the spectrum of *trans*-MMA.

1. The trans conformer

As a first step, we neglected the methyl internal rotation and treated *trans*-MMA as an effective rigid-rotor. A spectrum containing A species transitions was predicted with the program *XIAM* in its rigid-rotor mode using the rotational constants given in Sec. II A 1 and was compared with the experimental broadband scan mentioned in Sec. III A. The very intense *R*-branch $J = 6 \leftarrow 5$ and $7 \leftarrow 6$ *a*-type transitions with $K_a = 0$ and 1 were firstly identified in the scan, yielding the *B* and *C* rotational constants. Afterwards, *b*-type transitions were also assigned, which fixed the *A* rotational constant. This enabled a prediction of the whole rigid-rotor spectrum with sufficient accuracy to find all the remaining A species lines in the frequency range of 2-26.5 GHz. At this stage, 183 lines were fitted with the three rotational constants *A*, *B*, and *C* and five quartic centrifugal distortion constants.

As a next step, we took into account the methyl internal rotation and predicted both the A and E species transitions. The initial V_3 potential and the angle between the internal rotor axis and the principal *a*-axis were taken from quantum chemical calculations. By comparing the theoretical and experimental broadband scan, the assignment was straightforward for the *a*-type *R*-branch transitions mentioned above, where the A-E splittings were less than 30 MHz. The assignment of *b*-type lines with much larger splittings (up to 3.5 GHz) was more difficult, however, finally successful. In total, 183 A species and 137 E species lines were fitted using the program *XIAM* with a standard deviation of 32.1 kHz. The molecular parameters are summarized as Fit I in Table II. A list including all the fitted transitions is given in Table S3 (supplementary material).

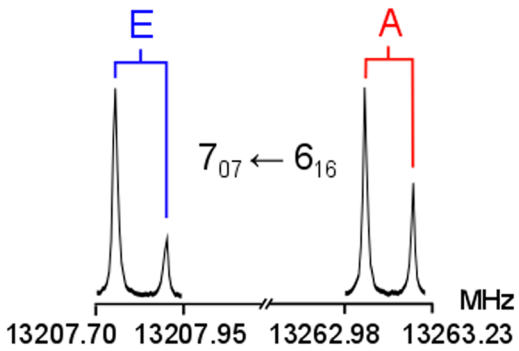

FIG. 6. A typical spectrum of the $7_{07} \leftarrow 6_{16}$ transition of the *cis* conformer of MMA with its A and E torsional species. The A-E splitting is approximately 55 MHz. The splittings indicated by brackets are due to the Doppler effect. For each of these spectra, 50 decays were co-added.

2. The cis conformer

After the *trans* conformer was assigned, a large number of lines remained in the scan, which belong to the *cis* conformer. Because only *b*-type transitions are present (see Sec. II A 1), the assignment was more difficult, nevertheless, possible by trial and error. We could measure and fit 92 A species and 131 E species transitions up to $J = 13$ with the program *XIAM* to a standard deviation of 27.0 kHz. This fit is also given in Table II; the fitted transitions are presented in Table S4 (supplementary material). We note that for both conformers, some *c*-type transitions are available in the frequency lists [Tables S3 and S4 (supplementary material)], which are all E species lines. It is known that for the E species, forbidden transitions can be observed,[3] as found, e.g., in ethyl acetate[34] and butadienyl acetate.[35]

3. The aixPAM fits

As mentioned above, *aixPAM* was written to check the accuracy of *XIAM*. It is a very flexible code in which effective terms can easily be added in the Hamiltonian. We made the following two sample calculations.

(1) We took the same MMA data set and the same set of parameters mentioned in Secs. III B 1 and III B 2 for comparative fits with *XIAM* and *aixPAM*. These *aixPAM* fits are given as Fit II in Table II. The D_{pi2} parameters often used in *XIAM* are also floated in *aixPAM*, where D_{pi2J} multiplies $2(p_\alpha - \vec{\rho}^\dagger\vec{P})^2\vec{P}^2$, D_{pi2K} multiplies $\{(p_\alpha - \vec{\rho}^\dagger\vec{P})^2, P_z^2\}$, and D_{pi2-} multiplies $\{(p_\alpha - \vec{\rho}^\dagger\vec{P})^2, (P_x^2 - P_y^2)\}$. The anti-commutator is defined as $\{u, v\} = uv + vu$; $\vec{\rho}^\dagger$ is the transposed rho vector. The complete definitions in terms of *aixPAM*'s fundamental operators are extensive and therefore given in Table S5 (supplementary material).

The standard deviations are very similar in both the fits. The one obtained from *aixPAM* is only slightly better than that from *XIAM* by about 4 kHz, indicating that the matrix elements neglected in *XIAM* do not significantly limit its accuracy. The observed-minus-calculated values of Fit II are listed in Table S3 (supplementary material) for *trans*-MMA and in Table S4 (supplementary material) for *cis*-MMA.

(2) We added in a second *aixPAM* fit some effective terms not available in *XIAM*. This enabled us to achieve a standard deviation close to the experimental accuracy. For *cis*-MMA, three additional parameters V_J multiplying $P^2(1 - \cos 3\alpha)$, D_{mK} multiplying $P_z{}^2 p_\alpha{}^2$, and

TABLE II. Molecular parameters of *m*-methylanisole in the principal axis system obtained by the programs *XIAM* and *aixPAM*.

		cis-MMA				*trans*-MMA			
Parameter[a]	Unit	Fit I[b]	Fit II[c]	Fit III[d]	Calculation[e]	Fit I[b]	Fit II[c]	Fit III[d]	Calculation[e]
A[f]	MHz	2755.8636(70)	2755.997(18)	2755.304(73)	2756.845	3529.454(40)	3528.242(61)	3521.824(85)	3537.943
B[f]	MHz	1293.7072(25)	1293.3105(60)	1291.236(45)	1286.597	1122.3350(17)	1122.3847(26)	1121.498(45)	1116.215
C[f]	MHz	890.60188(47)	890.55131(66)	890.88(16)	886.992	861.12564(46)	861.14249(47)	862.060(45)	857.656
Δ_J	kHz	0.0421(31)	0.0493(26)	0.05137(42)	0.05173	0.0310(33)	0.0285(29)	0.02397(43)	0.02326
Δ_{JK}	kHz	−0.027(22)	−0.076(19)	−0.0951(31)	−0.06667	0.071(21)	0.034(19)	0.0451(28)	0.09015
Δ_K	kHz	0.601(99)	0.542(85)	0.446(14)	0.39097	−0.478(94)	0.299(84)	0.954(15)	0.57448
δ_J	kHz	0.0129(14)	0.0169(12)	0.01833(19)	0.01869	0.0091(17)	0.0085(15)	0.00609(22)	0.00598
δ_K	kHz	0.045(16)	0.101(13)	0.0846(21)	0.04213	0.119(57)	0.134(51)	0.0857(75)	0.00370
D_{pi2J}	kHz	93.10(87)	97.68(85)	157.8(59)		−34.80(46)	−34.64(42)	−64.99(65)	
D_{pi2K}	MHz	−0.2333(43)	−0.1864(43)	−0.4450(33)		0.904(22)	0.996(21)	1.2828(85)	
D_{pi2-}	kHz	66.34(84)	75.72(83)	161.4(66)		−20.56(48)	−18.01(44)	49.9(36)	
V_3	cm^{-1}	55.784(34)	55.469(34)	55.7693(90)	50.128	36.548(32)	36.392(32)	36.6342(84)	32.768
F_0	GHz	157.074(96)	156.190(96)	157.192(28)	160.898	158.10(15)	157.45(14)	158.825(38)	160.855
V_J	MHz	...	...	1.41(12)		...	...	...	
D_{mK}	MHz	...	...	0.4122(59)		...	...	...	
V_K	MHz	...	...	...		...	...	9.97(12)	
V_-	MHz	...	...	1.92(13)		...	...	1.265(61)	
D_{mJ}	MHz	...	...	...		...	...	0.0491(12)	
∠(i,a)	deg	51.6451(1)	51.65520(20)	51.6942(12)	52.140	146.8215(1)	146.83013(53)	146.8552(14)	146.887
∠(i,b)	deg	141.6451(1)	141.65520(20)	141.6942(12)	142.140	123.1785(1)	123.16987(53)	123.1448(14)	123.113
∠(i,c)	deg	90.0[g]	90.0[g]	90.0[g]	89.996	90.0[g]	90.0[g]	90.0[g]	89.995
N_A/N_E[h]		92/131	92/131	92/131		183/137	183/137	183/137	
σ[i]	kHz	27.0	23.0	3.7		32.1	28.3	4.1	

[a]All parameters refer to the principal axis system. Watson's A reduction and I^r representation were used.
[b]Fit with the program *XIAM*.
[c]Fit with the program *aixPAM* using the same parameters as in Fit I.
[d]Fit with the program *aixPAM* using three additional parameters.
[e]Centrifugal distortion constants obtained from anharmonic frequency calculations; all other values from geometry optimizations at the B3LYP/6-311++G(d,p) level of theory.
[f]Derived from the linear combinations $B_J = ½ (B + C)$, $B_K = A - ½ (B + C)$, and $B_- = ½ (B - C)$. The standard errors of A, B, and C were obtained from $\sigma_A = \sqrt{\sigma_{BJ}^2 + \sigma_{BK}^2 + 2\rho_{BJ,BK}\sigma_{BJ}\sigma_{BK}}$, $\sigma_B = \sqrt{\sigma_{BJ}^2 + \sigma_{B-}^2 + 2\rho_{BJ,B-}\sigma_{BJ}\sigma_{B-}}$, and $\sigma_C = \sqrt{\sigma_{BJ}^2 + \sigma_{B-}^2 - 2\rho_{BJ,B-}\sigma_{BJ}\sigma_{B-}}$, respectively, with the correlation coefficients $\rho_{BJ,BK}$ and $\rho_{BJ,B-}$.
[g]Fixed due to symmetry.
[h]Number of the A and E species lines.
[i]Standard deviation of the fit. All fits were carried out with a basis size $k_{max} = 8$.

V_- multiplying $(P_x^2 - P_y^2)(1 - \cos 3\alpha)$ lowered the standard deviation to 3.7 kHz, which is the measurement accuracy. For *trans*-MMA, the standard deviations were reduced to 4.1 kHz by adding the parameters V_K multiplying $P_z^2(1 - \cos 3\alpha)$, D_{mJ} multiplying $P^2 p_\alpha^2$, and V_-, where in both cases, the operators containing the $(1 - \cos 3\alpha)$ term led to the most significant changes of the fits. It should be noted that the RAM equivalent versions of these operators are also available in *BELGI*. These *aixPAM* fits are summarized as Fit III in Table II.

IV. DISCUSSION

While no significant differences between Fit I and Fit II are observed, Fit III in Table II shows that *aixPAM* improves the standard deviations for both the *trans* and *cis* conformers of MMA, to measurement accuracy by adding three parameters in the fits. Therefore, we assumed that additional effective parameters in *XIAM* would allow fits with standard deviations close to those obtained with *aixPAM* or *BELGI*. The torsional barriers of the ring methyl group of 36.6342(84) cm^{-1} (*trans*-MMA) and 55.7693(90) cm^{-1} (*cis*-MMA), according to Fit III, are significantly different. Compared with the barrier heights of 444 cm^{-1} and 50 cm^{-1} observed for OMA[17] and PMA,[18] respectively, it is deduced that the V_3 potential changes for each isomer because the methyl rotor encounters different local environments. The same effect was observed in other toluene derivatives, as indicated in Table III.

The torsional barriers of the *o*-isomers are largest, because the barrier heights are dominated by steric hindrance, since the substituents are adjacent to each other in the benzene ring. The barriers decrease in *m*-isomers, because the substituents are further apart, which creates a symmetric local environment near the methyl group, even though the global frame of the molecule is still asymmetric. The *p*-isomers often possess the smallest barriers,[18,24,26] because the molecule is electronically and structurally symmetric, as already discussed in Ref. 18.

In OMA, only one conformer exists, with the methoxy methyl group pointing away from the methyl group, since steric effects predominate any stabilization due to six-membered ring interaction.[17] Conversely, the distance between the substituents of MMA is large enough to negate steric hindrance, leading to two stable conformers. In PMA, the

TABLE III. Torsional barriers of toluene derivatives in cm^{-1}.

Molecule	*ortho*	*cis-meta*	*trans-meta*	*para*
Tolunitrile	187.699(3)[36]	14.1960(3)[a,37]		...[b]
Fluorotoluene	227.28(2)[19]	15.8(1.1)[a,20]		4.8298(64)[b,21]
^{35}Cl-chlorotoluene	513.8(27)[38]	...[a]		4.872(14)[b,c,39]
Xylene	518.3(32)[40]	4.49(14)[a,41]		...
Cresol	371.05(41)[d,22]	22.44(7)[23]	3.2(2)[23]	18.39(3)[24]
Methylbenzaldehyde	...	35.925(3)[25]	4.64(3)[25]	28.37[26]
Methylanisole	444.48(42)[17]	55.7693(90)[e]	36.6342(84)[e]	49.6370(1)[18]

[a]Only one conformer due to symmetry of the *m*-substituent.
[b]Only V_6 potential exists due to symmetry.
[c]Value determined by initial defect.
[d]Value for the *anti* conformer. The respective value for the *syn* conformer is 669.10(51) cm^{-1}.
[e]This work.

symmetry of the molecule allows for only one conformer.[18] Only few examples are reported in the literature concerning the conformational effect on torsional barriers. The studies on *m*-cresol, *m*-methylbenzaldehyde, and MMA (this work) have explored significant differences in the V_3 potentials between the rotational conformers, where in all cases, the barrier for the *trans* conformer is lower. As discussed in Ref. 35, there are two factors that affect the height of a methyl rotor torsional barrier: steric hindrance and electronic configuration. In the *m*-substituted toluenes mentioned, steric effects are absent and the far distance between the two substituents implies that electronic properties are more likely responsible for the different barrier heights.

In the case of *o*-cresol, where exceptionally both *anti* (*trans*) and *syn* (*cis*) conformers exist because of the low steric hindrance of the OH group, the barrier of 371.05(41) cm^{-1} found for *anti-o*-cresol is also much lower than that of 669.10(51) cm^{-1} found for *syn-o*-cresol. However, because the hydroxy and the ring methyl group are close in *syn-o*-cresol, this observation can still be explained by steric effects.

Alvarez-Valtierra *et al.* have already reported on the internal rotation of the ring methyl group in MMA with V_3 potentials of 57.07 cm^{-1} (*cis*-MMA) and 30.35 cm^{-1} (*trans*-MMA) using fluorescence spectroscopy.[42] In comparison with the microwave spectroscopic data, for *cis*-MMA, the values are consistent within a small difference of 1.3 cm^{-1}. For *trans*-MMA, the barrier height obtained from fluorescence spectroscopy differs by more than 6 cm^{-1} from that determined by microwave spectroscopy.[42] Not only the torsional barriers but also the rotational constants do not match in studies by microwave and fluorescence spectroscopy, as indicated in Table IV. We believe that molecular parameters obtained by microwave spectroscopy are more accurate and reliable because of its higher resolution than that of fluorescence spectroscopy.

TABLE IV. Comparison of the rotational constants *A*, *B*, and *C* (in MHz) as well as the V_3 potential (in cm^{-1}) of *m*-methylanisole observed by microwave spectroscopy (Fit III in Table II) and fluorescence spectroscopy (Fit F).[42]

Parameter	Fit F	Fit III	Fit III – Fit F
cis-MMA			
A	2766.7(1)	2755.304(73)	−11.4
B	1297.5(1)	1291.236(45)	−6.3
C	890.7(1)	890.88(16)	0.2
V_3	57.07	55.7693(90)	−1.30
trans-MMA			
A	3573.1(1)	3521.824(85)	−51.3
B	1124.2(1)	1121.498(45)	−2.7
C	861.1(1)	862.060(45)	1.0
V_3	30.35	36.6342(84)	6.28

Structural parameters such as rotational constants and the angles between the internal rotor axis and the principal axes as well as the V_3 barrier height calculated at the B3LYP/6-311++G(d,p) level of theory agree well with the experimental values for two conformers of MMA (see Table II). Centrifugal distortion constants predicted by anharmonic frequency calculations are in the same order of magnitude with the experimental values. Therefore, we conclude that the B3LYP/6-311++G(d,p) level is sufficiently suited for optimizing the structures of MMA.

Finally, after the spectra of *cis*- and *trans*-MMA were assigned, no intense lines remain in the broadband scan (see Fig. 5), implying that ^{13}C isotopologues or water complexes are not observable for this compound under our measurement conditions.

SUPPLEMENTARY MATERIAL

See supplementary material for the Fourier coefficients of the potential functions, Cartesian coordinates, frequency lists, definitions of some operators, and correlation matrices of the fits.

ACKNOWLEDGMENTS

We thank the Land Nordrhein-Westfalen for funds. Simulations were performed with computing resources granted by RWTH Aachen University under Project No. <thes0248>.

[1]R. C. Woods, J. Mol. Spectrosc. **22**, 49 (1967).
[2]H. Hartwig and H. Dreizler, Z. Naturforsch., A **51**, 923 (1996).
[3]J. T. Hougen, I. Kleiner, and M. Godefroid, J. Mol. Spectrosc. **163**, 559 (1994).
[4]I. Kleiner and J. T. Hougen, J. Chem. Phys. **119**, 5505 (2003).
[5]P. Groner, J. Chem. Phys. **107**, 4483 (1997).
[6]V. V. Ilyushin, Z. Kisiel, L. Pszczółkowski, H. Mäder, and J. T. Hougen, J. Mol. Spectrosc. **259**, 26 (2010).
[7]C. C. Lin and J. D. Swalen, Rev. Mod. Phys. **31**, 841 (1959).

[8]A. O. Hernandez-Castillo, C. Abeysekera, B. M. Hays, I. Kleiner, H. V. L. Nguyen, and T. S. Zwier, J. Mol. Spectrosc. **337**, 51 (2017).
[9]R. Kannengießer, S. Klahm, H. V. L. Nguyen, A. Lüchow, and W. Stahl, J. Chem. Phys. **141**, 204308 (2014).
[10]Y. Zhao, W. Stahl, and H. V. L. Nguyen, Chem. Phys. Lett. **545**, 9 (2012).
[11]K. Eibl, R. Kannengießer, W. Stahl, H. V. L. Nguyen, and I. Kleiner, Mol. Phys. **114**, 3483 (2016).
[12]H. V. L. Nguyen, H. Mouhib, W. Stahl, and I. Kleiner, Mol. Phys. **108**, 763 (2010).
[13]R. Kannengießer, M. J. Lach, W. Stahl, and H. V. L. Nguyen, ChemPhysChem **16**, 1906 (2015).
[14]R. Kannengießer, W. Stahl, H. V. L. Nguyen, and I. Kleiner, J. Phys. Chem. A **120**, 3992 (2016).
[15]H. V. L. Nguyen, A. Jabri, V. Van, and W. Stahl, J. Phys. Chem. A **118**, 12130 (2014).
[16]L. Sutikdja, W. Stahl, V. Sironneau, H. V. L. Nguyen, and I. Kleiner, Chem. Phys. Lett. **663**, 145 (2016).
[17]L. Ferres, H. Mouhib, W. Stahl, and H. V. L. Nguyen, ChemPhysChem **18**, 1855 (2017).
[18]L. Ferres, W. Stahl, I. Kleiner, and H. V. L. Nguyen, J. Mol. Spectrosc. **343**, 44 (2018).
[19]S. Jacobsen, U. Andresen, and H. Mäder, Struct. Chem. **14**, 217 (2003).
[20]H. D. Rudolph and A. Trinkaus, Z. Naturforsch., A **23**, 68 (1968).
[21]J. Rottstegge, H. Hartwig, and H. Dreizler, J. Mol. Struct. **478**, 37 (1999).
[22]A. Welzel, A. Hellweg, I. Merke, and W. Stahl, J. Mol. Spectrosc. **215**, 58 (2002).
[23]A. Hellweg, C. Hättig, I. Merke, and W. Stahl, J. Chem. Phys. **124**, 204305 (2006).
[24]A. Hellweg and C. Hättig, J. Chem. Phys. **127**, 024307 (2007).
[25]A. J. Shirar, D. S. Wilcox, K. M. Hotopp, G. L. Storck, I. Kleiner, and B. C. Dian, J. Phys. Chem. A **114**, 12187 (2010).
[26]H. Saal, J.-U. Grabow, A. Hight-Walker, J. T. Hougen, W. Caminati, and I. Kleiner, in 65th Ohio State University International Symposium on Molecular Spectroscopy, Columbus, Ohio, USA, June 2010, presentation #WH07.
[27]M. J. Frisch, G. W. Trucks, H. B. Schlegel, G. E. Scuseria, M. A. Robb, J. R. Cheeseman, G. Scalmani, V. Barone, B. Mennucci, G. A. Petersson, H. Nakatsuji, M. Caricato, X. Li, H. P. Hratchian, A. F. Izmaylov, J. Bloino, G. Zheng, J. L. Sonnenberg, M. Hada, M. Ehara, K. Toyota, R. Fukuda, J. Hasegawa, M. Ishida, T. Nakajima, Y. Honda, O. Kitao, H. Nakai, T. Vreven, J. A. Montgomery, Jr., J. E. Peralta, F. Ogliaro, M. Bearpark, J. J. Heyd, E. Brothers, K. N. Kudin, V. N. Staroverov, R. Kobayashi, J. Normand, K. Raghavachari, A. Rendell, J. C. Burant, S. S. Iyengar, J. Tomasi, M. Cossi, N. Rega, J. M. Millam, M. Klene, J. E. Knox, J. B. Cross, V. Bakken, C. Adamo, J. Jaramillo, R. Gomperts, R. E. Stratmann, O. Yazyev, A. J. Austin, R. Cammi, C. Pomelli, J. W. Ochterski, R. L. Martin, K. Morokuma, V. G. Zakrzewski, G. A. Voth, P. Salvador, J. J. Dannenberg, S. Dapprich, A. D. Daniels, O. Farkas, J. B. Foresman, J. V. Ortiz, J. Cioslowski, and D. J. Fox, GAUSSIAN 09, Revision A.02, Gaussian, Inc., Wallingford, CT, 2009.
[28]L. Ferres, W. Stahl, and H. V. L. Nguyen, Mol. Phys. **114**, 2788 (2016).
[29]V. Van, W. Stahl, and H. V. L. Nguyen, Phys. Chem. Chem. Phys. **17**, 32111 (2015).
[30]V. Van, W. Stahl, and H. V. L. Nguyen, ChemPhysChem **17**, 3223 (2016).
[31]D. Moran, A. C. Simmonett, F. E. Leach, W. D. Allen, P. V. R. Schleyer, and H. F. Schaefer, J. Am. Chem. Soc. **128**, 9342 (2006).
[32]H. Dreizler, Fortschr. Chem. Forsch. **10**, 59 (1968).
[33]J.-U. Grabow, W. Stahl, and H. Dreizler, Rev. Sci. Instrum. **67**, 4072 (1996).
[34]D. Jelisavac, D. C. Cortés-Gómez, H. V. L. Nguyen, L. W. Sutikdja, W. Stahl, and I. Kleiner, J. Mol. Spectrosc. **257**, 111 (2009).
[35]A. Jabri, V. Van, H. V. L. Nguyen, W. Stahl, and I. Kleiner, ChemPhysChem **17**, 2660 (2016).
[36]N. Hansen, H. Mäder, and T. Bruhn, Mol. Phys. **97**, 587 (1999).
[37]T. Bruhn and H. Mäder, J. Mol. Spectrosc. **200**, 151 (2000).
[38]K. P. R. Nair, J. Demaison, G. Wlodarczak, and I. Merke, J. Mol. Spectrosc. **237**, 137 (2006).
[39]G. E. Herberich, Z. Naturforsch., A **22**, 761 (1967).
[40]H. D. Rudolph, K. Walzer, and I. Krutzik, J. Mol. Spectrosc. **47**, 314 (1973).
[41]C. Thomsen and H. Dreizler, Z. Naturforsch., A **56**, 635 (2001).
[42]L. Alvarez-Valtierra, J. T. Yi, and D. W. Pratt, J. Phys. Chem. B **110**, 19914 (2006).